Mode-locking and frequency mixing at THz pulse repetition rates in a sampled-grating DBR mode-locked laser

Lianping Hou,* Mohsin Haji, and John H. Marsh

School of Engineering, University of Glasgow, G12 8LT, Glasgow, UK
lianping.hou@glasgow.ac.uk

Abstract: We report a sampled grating distributed Bragg reflector (SGDBR) laser with two different gratings which mode-lock independently at respective pulse repetition frequencies of 640 and 700 GHz. The device operates in distinct regimes depending on the bias conditions, with stable pulse trains observed at 640 GHz, 700 GHz, the mean repetition frequency of 666 GHz, and the sum frequency of 1.34 THz (due to nonlinear mixing). Performance is consistent and highly reproducible with exceptional stability observed over wide ranges of drive bias conditions. Furthermore, a monolithically integrated semiconductor optical amplifier is used to amplify the pulse trains, providing an average output power of 46 mW at 666 GHz.

OCIS codes: (140.4050) Mode-locked lasers; (230.1480) Bragg reflectors; (250.5980) Semiconductor optical amplifiers; (190.4223) Nonlinear wave mixing; (320.7090) Ultrafast lasers.

References and links

1. E. L. Portnoi and A. V. Chelnokov, "Passive mode-locking in a short cavity laser," in Dig. 12th IEEE Semiconductor Conf., Davos, Switzerland, 140–141 (1990).
2. Y. Wen, D. Novak, H. Liu, and A. Nirmalathus, "Generation of 140GHz optical pulses with suppressed amplitude modulation by subharmonic synchronous mode locking of Fabry-Perot semiconductor laser," Electron. Lett. **37**(9), 581–582 (2001).
3. T. Shimizu, I. Ogura, and H. Yokoyama, "860 GHz rate asymmetric colliding pulse mode locked diode lasers," Electron. Lett. **33**(22), 1868–1869 (1997).
4. S. Arahira, Y. Matsui, and Y. Ogawa, "Mode-locking at very high repetition rates more than terahertz in passively mode-locked distributed-Bragg-reflector laser diodes," IEEE J. Quantum Electron. **32**(7), 1211–1224 (1996).
5. D. A. Yanson, M. W. Street, S. D. McDougall, I. G. Thayne, J. H. Marsh, and E. A. Avrutin, "Ultrafast Harmonic Mode-Locking of Monolithic Compound-Cavity Laser Diodes Incorporating Photonic-Bandgap Reflectors," IEEE J. Quantum Electron. **38**(1), 1–11 (2002).
6. L. Hou, R. Dylewicz, M. Haji, P. Stolarz, B. Qiu, and A. C. Bryce, "Monolithic 40 GHz passively mode-locked AlGaInAs/InP 1.55 μm MQW laser with surface-etched distributed Bragg reflector," IEEE Photon. Technol. Lett. **22**(20), 1503–1505 (2010).
7. M. Tani, P. Gu, M. Hyodo, K. Sakai, and T. Hidaka, "Generation of coherent terahertz radiation by photomixing of dual-mode lasers," Opt. Quantum Electron. **32**(4/5), 503–520 (2000).
8. Z. Yang, L. Mutter, M. Stillhart, B. Ruiz, S. Aravazhi, M. Jazbinsek, A. Schneider, V. Gramlich, and P. Günter, "Large-size bulk and thin-film stilbazolium-salt single crystals for nonlinear optics and THz generation," Adv. Funct. Mater. **17**(13), 2018–2023 (2007).
9. L. Hou, P. Stolarz, J. Javaloyes, R. Green, C. N. Ironside, M. Sorel, and A. C. Bryce, "Subpicosecond pulse generation at quasi-40-GHz using a passively mode locked AlGaInAs/InP 1.55 μm strained quantum well laser," IEEE Photon. Technol. Lett. **21**(23), 1731–1733 (2009).
10. V. Jayaraman, Z. M. Chuang, and L. A. Coldren, "Theory, design, and performance of extended tuning range semiconductor lasers with sample gratings," IEEE J. Quantum Electron. **29**(6), 1824–1834 (1993).
11. B. W. Hakki and T. L. Paoli, "Gain spectra in GaAs double-heterostructure injection lasers," J. Appl. Phys. **46**(3), 1299–1305 (1975).
12. M. C. Aman and J. Buus, "Tunable semiconductor lasers," Astech House, Norwood, MA, 1998.
13. L. Hou, M. Haji, J. Akbar, and J. H. Marsh, "Narrow linewidth laterally-coupled 1.55μm AlGaInAs_InP DFB laser integrated with a curved tapered SOA," Opt. Lett. **37**(21), 4525–4527 (2012).
14. J. Fricke, H. Wenzel, M. Matalla, A. Klehr, and G. Erbert, "980-nm DBR lasers using higher order gratings defined by i-line lithography," Semicond. Sci. Technol. **20**(11), 1149–1152 (2005).

#213508 - $15.00 USD Received 6 Jun 2014; revised 20 Aug 2014; accepted 21 Aug 2014; published 29 Aug 2014

15. G. P. Agrawal and N. A. Olsson, "Self-phase modulation and spectral broadening of optical pulses in semiconductor laser amplifier," IEEE J. Quantum Electron. **25**(11), 2297–2306 (1989).
16. S. Spiessberger, M. Schiemangk, A. Wicht, H. Wenzel, O. Brox, and G. Erbert, "Narrow linewidth DFB lasers emitting near a wavelength of 1064 nm," J. Lightwave Technol. **28**(17), 2611–2616 (2010).

1. Introduction

Ultrafast mode-locked laser (MLL) diodes offer exciting opportunities in future telecoms systems, high speed data processing and miniaturized THz signal generators because they are compact, robust, cheap to manufacture, and can be integrated with other semiconductor elements such as semiconductor optical amplifiers (SOAs). For a laser diode (LD) with a typical cavity length between 0.5 and 1 mm, the corresponding mode-locking (ML) frequency is around 80 to 170 GHz [1]. One of the distinct ways of achieving higher ML frequencies is to introduce harmonic mode-locking (HML) techniques. A HML laser produces an optical pulse train at an integer multiple of the fundamental round-trip frequency of the device, which can be achieved using sub-harmonic optical injection [2], colliding pulse ML (CPM) [3], or compound-cavity ML (CCM) methods [4, 5]. Frequencies of up to 1.5 THz have been achieved with the use of CCM effects in distributed Bragg reflector (DBR) lasers [4], albeit operating over a narrow range of bias conditions and with limited reproducibility. The most extensive demonstration of HML used purpose-built AlGaAs/GaAs CCM Fabry-Perot (FP) lasers incorporating an intra-cavity reflector (ICR), where repetition frequencies up to 2.1 THz were demonstrated at 850 nm [5]. However, despite this record-high frequency achievement, the reported laser cannot benefit from the use of erbium-doped fiber amplifiers (EDFAs) for subsequent amplification. For both CPM and CCM based lasers, the cavity cleaving accuracy is critical for adequate HML to occur. In the case of the CCM laser described in [5], the accuracy of the positioning of the ICR within the cavity was decisive in determining the ML frequency, and the fabrication processes required to create a high quality deep etched ICR are relatively complicated and challenging. These tight tolerances arise from the fact that the FP cavities are used both as frequency filters, generating a comb of equally spaced longitudinal resonances, and as the spatial cavities around which the pulses circulate. For the CCM laser [5], this means that the length of the long cavity must be an exact integer multiple, with a very tight tolerance, of that of the short cavity. If there is a small mismatch in the cavity lengths, periodic modulation signatures can be seen in the pulse stream, and furthermore when there is a larger mismatch ML may not occur at all, especially in lasers operating at 1.5 μm.

In this paper we describe a sampled-grating DBR (SGDBR) MLL integrated with a SOA. The front and rear DBR sections each act as optical filters to independently mode-lock the laser at different sub-THz frequencies (640 GHz and 700 GHz, respectively) and hence generate optical signals modulated at their respective ML frequencies. When the optical modes are broadened, a pulse train at the mean value of the rear and front SGDBR frequencies is produced, whilst nonlinear mixing, primarily in the SA, gain and SOA sections, results in a pulse train at the sum of the mixed frequencies, i.e. 1.34 THz.

All of these frequency mixing features can be well controlled by adjusting the bias conditions, and the devices offer far superior reproducibility and a operate over a wider range of bias conditions than all other reported mode-locked THz LDs [4, 5]. This exceptional performance compared to FP MMLs is fundamentally due to the precise selection of modal frequencies which are accurately determined in absolute frequency and frequency spacing by the front and rear SGDBR sections. Furthermore, pulses are reflected into the main cavity from along the distributed length of the grating; provided the grating is sufficiently long, the laser is able to self adjust so that the spectral resonances of each of the SGDBRs align with a subset of the resonant frequencies of the main cavity. This mechanism does not depend on cleaving and is therefore more robust in manufacture. Additionally, in contrast to the complex fabrication processes used for conventional DBR lasers, those based on side-wall gratings offer advantages such as simpler regrowth-free fabrication and increased design flexibility. The DBR can be simultaneously lithographically patterned and etched along with the ridge waveguide, reducing the number of fabrication steps. The regrowth-free approach enables Al-

#213508 - $15.00 USD Received 6 Jun 2014; revised 20 Aug 2014; accepted 21 Aug 2014; published 29 Aug 2014

containing epitaxial layers to be used, as there is no exposure of surfaces containing Al, which can oxidize and cause problems during epitaxial regrowth [6]. The results presented in this article suggest that our device could be used as a compact, stable, solid-state practical laser source for generating THz radiation using a photoconductive antenna [7] or nonlinear optical crystal [8].

2. Device structure and fabrication

The epitaxial structure is the same as that described in [9]. An optical microscope photo of the top view (p-side) of the fabricated device along with its dimensions is shown in Fig. 1(a). The device has a total cavity length of 3592 μm of which the gain section is 1580 μm, the SA section is 30 μm, the front SGDBR section is 492 μm, and the rear SGDBR is 810 μm long. The ridge waveguide width (w) is 2.5 μm. The curved SOA is 600 μm long with a curvature radius of 3455 μm, and a tilt of 10° at the output facet, forming an SOA segment used to boost the output power on-chip. Electrical isolation between the electrodes was obtained by wet-etching slots 20 μm wide and 250 nm deep in the contact layer. The relatively short length SA section is used to facilitate adequate short-pulse generation from self-colliding propagating pulses.

The SGDBR sections use a side-wall grating as shown schematically in Fig. 1(b), where Z_0 represents the burst period of the grating. The ML frequency is then given by $F_r = c/(2n_gZ_0)$, where c is the velocity of light in free space, n_g is the group index. Z_0 for the rear and front SGDBR is 67.5 μm and 61.5 μm, respectively. The rear and front SGDBRs were designed to spectrally select longitudinal modes with the precise mode spacings required to generate signals at F_r = 0.64 THz and 0.7 THz, respectively. Z_1 represents the length of the grating burst, which is 10 μm long and of first-order with a 50% duty cycle and formed by etching 0.6 μm deep recesses (d) into the sidewalls of the waveguide for both the front and rear SGDBRs [inset in Fig. 1(b)]. Λ represents the grating period and is 244 nm for a 1.55 μm Bragg wavelength. This operating wavelength was intentionally red-shifted from the photoluminescence (PL) wavelength of the quantum-well (QW) active layer at 1.53 μm in order to reduce the absorption loss in the SGDBR sections and enable them to work effectively as reflectors, even with the section unbiased or floating. The coupling coefficient of an unsampled grating, κ_0, was measured to be approximately 80 cm^{-1}. N_s represents the number of sample periods, and the SGDBR length (L_{sg}) is equal to $N_s \times Z_0$. The values of N_s for the front and rear SGDBR sections were 8 and 12 respectively, and were chosen to increase the reflectivity of the rear SGDBR relative to that of the front SGDBR in order to increase the output power of the signal emitted from the SOA side of the laser.

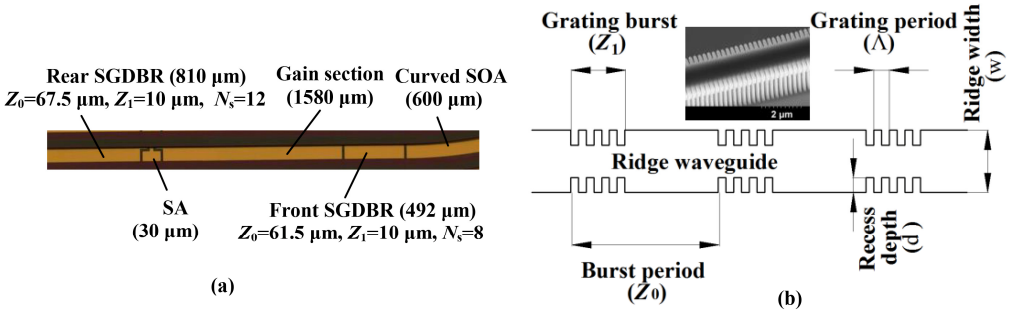

Fig. 1. (a) Optical microscope picture of the device, (b) schematic of the side-wall SGDBR and the inset shows the SEM picture of the side-wall grating burst of first-order with a 50% duty cycle and 0.6 μm depth recesses.

A schematic of the SGDBR MLL is shown in Fig. 2(a). The effective length of the main cavity ($L_{Eff\text{-}cav}$) is 1770 μm, which includes the SA and gain section cavities (L_{cav} = 1670 μm) and the effective lengths of the front and rear SGDBR sections. The gain section was pumped in order to provide sufficient material gain. A high reverse bias was applied to the SA section

#213508 - $15.00 USD Received 6 Jun 2014; revised 20 Aug 2014; accepted 21 Aug 2014; published 29 Aug 2014

to give an ideal mode locking SA with a fast recovery rate. The front and rear SGDBRs acted as mirrors with power reflectances of $R_{front\text{-}SGDBR}$ and $R_{rear\text{-}SGDBR}$, respectively. The effective lengths of the front and rear SGDBRs were much shorter than the 1770 μm effective cavity, at 40 μm and 60 μm, respectively, i.e., half of their grating length of L_{Fg} and L_{Rg} , which is equal to $N_s \times Z_1$ [10]. The net modal gain G_{net} is defined by the following equation:

$$G_{net} = \Gamma g - \left[\alpha + \frac{1}{2L_{Eff-cav}} \ln \left\{ \frac{1}{R_{rear-SGDBR} \cdot R_{front-SGDBR}} \right\} \right] \quad (1)$$

Where Γ is the optical confinement factor of the multi-quantum well (5%), g is the material gain per well, Γg is the modal gain, α is the internal loss (15/cm). The values of Γg and α (15/cm) were derived using the Hakki-Paoli method from the amplified spontaneous emission (ASE) spectrum emitted from a FP laser fabricated in the same wafer [11]. The calculated power reflection spectra of the rear and front SGDBRs, modeled using the transfer matrix method (TMM) [12] and taking into account the linear propagation loss with the DBR section unbiased (α = 15/cm), are shown in Fig. 2(b). The central peak wavelength (λ_{peak}) is at 1550 nm and the separations between reflectivity peaks are 5.1 nm and 5.6 nm for the rear and front SGDBR sections, respectively. The peak spacings correspond to the respective grating frequencies using: $(\lambda_{peak})^2/(2n_gZ_0)$, n_g = 3.4889. The total transmission (T) from the SOA output facet, which is calculated from the overall transfer matrix of $T_{tot} = M_{SOA} \times M_{Front\text{-}SGDBR} \times M_{Gain} \times M_{SA} \times M_{Rear\text{-}SGDBR}$, is shown in Fig. 2(c). Here we assume the modal gain Γg is 30/cm in the gain and SOA sections and the modal absorption loss is 400/cm in SA section (with a 2.9 V reverse voltage applied) and the internal loss α = 15/cm in the SGDBR sections. The reflections at both the rear-SGDBR and facets are considered negligible due to the end facet of the rear-SGDBR being significantly distant from the main effective cavity, and the reflectivity of the angled facet at the output of the SOA is < 0.1%. There are small features within the main peaks with a mode spacing of 0.190 nm which corresponds to the fundamental spacing of the main effective cavity length of 1770 μm, as shown in the inset of diagram of Fig. 2(a). This confirms the total output transmission consists of the product of the rear and front SGDBR reflectivities along with an overlaid modulation from the main cavity, which agrees well with the experimental results. Figure 2(d) shows the computed net gain spectrum of the ML-SGDBR LD according to Eq. (1). The gain shows periodical peaks with the periodicity determined by the reflection peaks of the rear (black) and front (red) SGDBRs. The rear SGDBR reflection peaks reside within the front SGDBR peaks, and the modes are reduced in amplitude which concurs with our measurement data (presented in Section 3). Due to the limited gain bandwidth, only the longitudinal modes, which are located in the part of the spectrum where the net gain is positive, will contribute to lasing and participate in ML. For simplicity, we did not take into account thermal effects when the gain and SOA sections were heavily pumped; this leads to a red-shift in wavelength as seen in our experimental results.

The device fabrication processes are similar to those described in [13], i.e. negative tone Hydrogen Silsequioxane (HSQ) was used both as an e-beam lithography resist and as a hard mask during reactive ion etching (RIE). HSQ was also used as the material for planarizing the 1.92 μm high ridge waveguide and SGDBR slots prior to depositing the metal contacts. The inset of Fig. 1(b) shows a scanning electron microscope (SEM) image of the side-wall grating, with excellent visibility of the mask transfer of the grating into the upper cladding layers. A good sidewall verticality of the etched region and little RIE lag at the foot of the gratings are plainly visible. As a final step, the sample was cleaved into individual laser bars with both facets left uncoated. The devices were mounted epitaxial layer-up on a copper heat sink which was affixed to a temperature controlled Peltier cooler. The heat sink temperature was maintained at 20 °C and the devices were tested under CW biasing conditions.

#213508 - $15.00 USD Received 6 Jun 2014; revised 20 Aug 2014; accepted 21 Aug 2014; published 29 Aug 2014

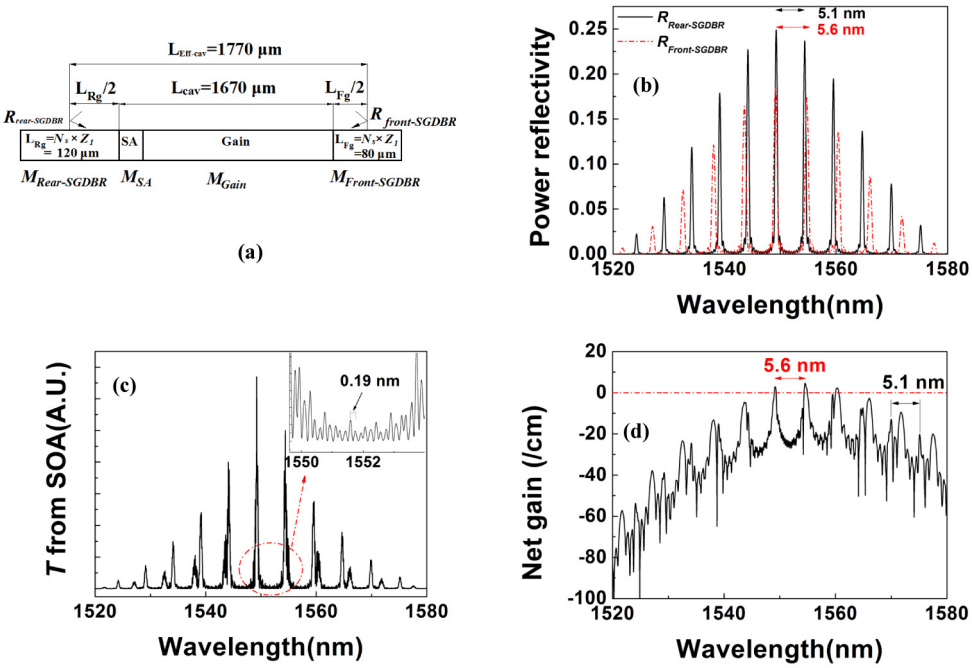

Fig. 2. (a) schematic of the experimental SGDBR MLL showing the effective length of the main cavity, rear and front SGDBR sections, (b) calculated power reflectivity of the rear and front SGDBRs, (c) calculated total transmission from the SOA output facet, the enlarged inset shows the internal fundamental mode spacing of 0.19 nm of the main cavity with an effective length of 1770 μm, (d) computed net gain of the ML-SGDBR LD which shows the wavelength peaks corresponding to reflections from the rear (black text) and front (red text) SGDBR segments.

3. Device performance

Figure 3(a) shows light-current (*L-I*) curves measured from the rear SGDBR output facet at different applied V_{SA} values (from 0 V to −3 V in steps of −0.5 V). The gain, front SGDBR, and SOA sections were left floating. The threshold current (I_{th}) was 50 mA at V_{SA} = 0 V. The change in the slope efficiency as the value of $|V_{SA}|$ was increased was almost imperceptible due to the position of the SA section at the rear SGDBR output facet, and thus having little effect on the output intensity. The maximum average output power was 8.65 mW for all investigated V_{SA} values at $I_{Rear\text{-}SGDBR}$ = 300 mA. Figure 3(b) shows the output power (*P*) measured from the facet on the SOA side as a function of I_{Gain} at different applied I_{SOA} values (from 0 to 350 mA in a step of 50 mA) with V_{SA} at −3.0 V, the front SGDBR current ($I_{Front\text{-}SGDBR}$) at 0 mA, and the rear SGDBR section left floating. For a fixed I_{SOA}, increasing I_{Gain} would, as expected, increase the output power from the SOA side facet. I_{th} was 80 mA.

Keeping I_{Gain} fixed while increasing I_{SOA} would also increase the output power as result of amplification in the SOA. When I_{SOA} was 350 mA, the SOA output reached saturation and further increases of the I_{SOA} caused a reduction of the output power due to heating. Compared with the results in Fig. 3(a), the SA absorption has an obvious effect on the output power from the SOA side facet, i.e. when increasing the value of applied $|V_{SA}|$, I_{th} increased and the slope efficiency reduced, thus the output power from the SOA side was smaller as a result. The maximum output powers when I_{SOA} = 350 mA, I_{Gain} = 300 mA for the cases of V_{SA} = 0 V, −2.0 V, and −3.0 V were 56 mW, 52 mW, 49 mW, respectively. Kinks were observed on some of the *L–I* curves, which are typical for a DBR laser and are caused by thermal detuning between the gain, SGDBR, and SOA sections, and are directly associated with the observed mode-hopping behavior [14].

#213508 - $15.00 USD Received 6 Jun 2014; revised 20 Aug 2014; accepted 21 Aug 2014; published 29 Aug 2014

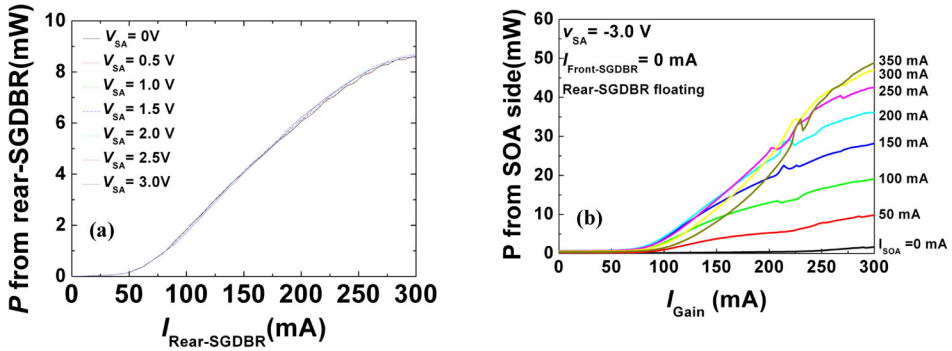

Fig. 3. (a) Output power from rear SGDBR side versus $I_{Rear\text{-}SGDBR}$ for different V_{SA} (from 0 V to −3 V in −0.5 V steps), the gain, front SGDBR, and SOA sections were floating. (b) Output power vs I_{Gain} for different I_{SOA} values (from 0 mA to 350 mA in 50 mA steps) for V_{SA} = −3.0 V with $I_{Front\text{-}SGDBR}$ = 0 mA, and rear SGDBR section floating.

3.1 Performance measured from rear SGDBR side with SOA sections floating

Firstly, we investigated the rear SGDBR characteristics by applying bias to this section and to the SA while the gain, front SGDBR, and SOA sections were left floating. In this scenario, ML operation at around 640 GHz pulse repetition frequency was realized over a large range of bias conditions (the current applied to the rear SGDBR section, $I_{Rear\text{-}SGDBR,}$ was varied from 240 mA to 300 mA, and V_{SA} from 0 V to −3.0 V).

Figure 4(a) shows the 2D optical spectral map over the range of $I_{Rear\text{-}SGDBR}$ from 0 mA to 300 mA with V_{SA} = −2.9 V and all other sections left floating. The spectra were measured with a resolution bandwidth (RBW) of 0.06 nm. From 30 mA up to the threshold current (50 mA), the rear SGDBR worked as a filter with equidistant peaks separated by 5.09 nm between the channels, consistent with the simulated results for the rear SGDBR shown in Fig. 2(b). From immediately above threshold up to 206 mA, the device behaved as an isolated distributed feedback (DFB) laser with a side-mode suppression ratio (SMSR) > 20 dB. This is due to the rest of the unbiased cavity absorbing the signal, limiting the reflections back to the forward biased rear SGDBR, and thus the majority of the light signal does not reach the SA for saturation to occur. When the gain current was > 240 mA, additional modes appeared in the optical spectrum (red lines in the Fig. 4(a)); the floating gain section, front SGDBR and even the SOA sections were sufficiently pumped by the rear SGDBR laser light to become almost transparent; therefore more light was reflected from the front SGDBR back to the rear SGDBR, reaching the SA and inducing the ML effect. Due to the reflection from the front SGDBR, even without an applied bias the presence of its mode spacing signature (yellow, i.e. low amplitude lines) was apparent close to the rear SGDBR modes (red, i.e. high amplitude lines) as evident in Fig. 4(a). For example, the optical spectrum at $I_{Rear\text{-}SGDBR}$ = 272 mA shows the longitudinal mode spacing of the rear SGDBR is around 0.48 nm or 58.2 GHz. The spacing of the main peak wavelengths of adjacent channels is non-equidistant, showing deviations of ± 2.5%. This is due to additional reflections from the front SGDBR, but all the peaks are present at precisely every 11th mode of the fundamental round-trip mode of the rear SGDBR, showing the mode spacing of the rear SGDBR is at a common “prime multiplier”. This is called partial HML, and in the time domain there would be several pulses with different amplitudes within the rear SGDBR cavity round-trip. The measured autocorrelation (AC) trace of the pulse train at $I_{Rear\text{-}SGDBR}$ = 272 mA is shown in Fig. 4(b), in which several pulses with different periods and amplitudes can be seen. The partial ML pulse average period is centred on 1.56 ps, corresponding to a partial ML pulse repetition frequency centred around 640 GHz.

Secondly, we investigated the device characteristics when the gain section was pumped and the front and rear SGDBR injection currents at 0 mA, with a reverse bias was applied to

#213508 - $15.00 USD Received 6 Jun 2014; revised 20 Aug 2014; accepted 21 Aug 2014; published 29 Aug 2014

the SA section and the SOA section left floating. In this scenario, the front and rear SGDBRs each acted as a passive filter with longitudinal mode spacings of 640 GHz and 700 GHz, respectively. Figure 4(c) shows the 2D optical spectral map over the range of I_{Gain} from 0 mA to 300 mA and $I_{Rear\text{-}SGDBR} = I_{Front\text{-}SGDBR} = 0$ mA with $V_{SA} = -2.2$ V and the SOA section left floating. Applying a bias between the threshold current of 80 mA and 300 mA produced some lower level peaks between the main peaks which were defined by the front SGDBR with its mode spacing of 700 GHz. These lower level peaks arose from reflections from both the rear and front SGDBRs, and are consistent with the simulation results presented in Fig. 2(c) and Fig. 2(d). Figure 4(d) shows the measured AC traces at $V_{SA} = -2.2$V, $I_{Rear\text{-}SGDBR} = I_{Front\text{-}SGDBR} = 0$ mA, $I_{Gain} = 280$ mA with the SOA section floating. The average pulse period is 1.4 ps, corresponding to a ML pulse repetition frequency around 700 GHz. There are clear additional frequency modulations observable in the AC traces, which correspond to the fundamental (around 24.3 GHz) and the second harmonic (around 48.6 GHz) round-tip frequencies of the 1770 μm long main effective cavity. The fundamental and second harmonic ML traces were observed in our experiments. This is discussed further in Section 3.2.

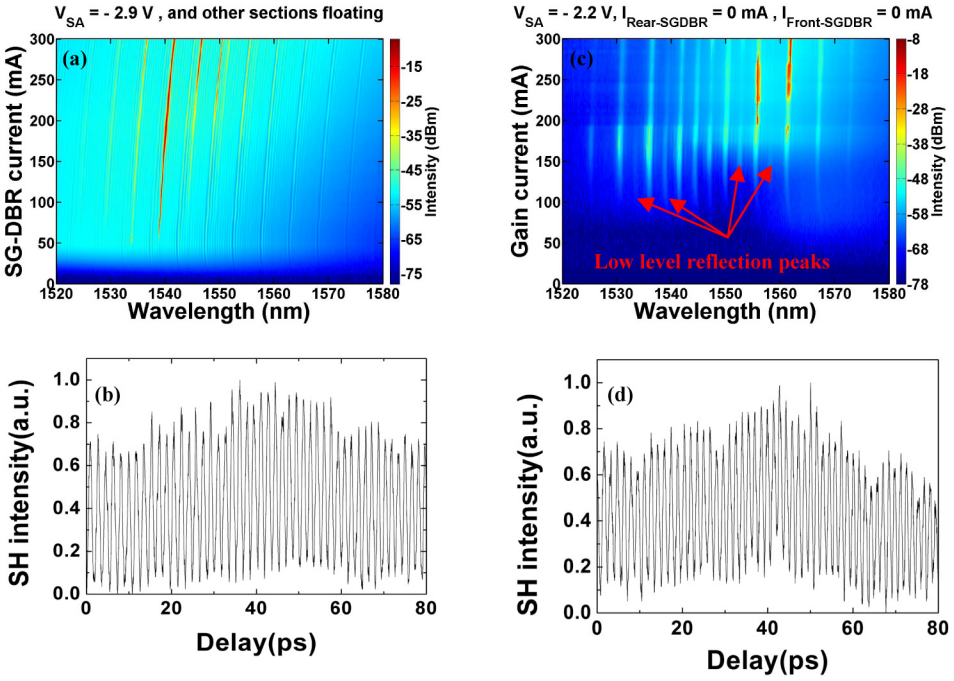

Fig. 4. Device performance measured from the rear SGDBR side output facet with $V_{SA} = -2.9$V and the gain, front SGDBR, and SOA sections floating: (a) 2D optical spectral map from the rear SGDBR side as a function of rear SGDBR current where the additional reflection peaks from the from SGDBR can be clearly seen, (b) corresponding autocorrelation traces with an average period of 1.56 ps at $I_{Rear\text{-}SGDBR} = 272$ mA. Device performance measured from the rear SGDBR side output facet with $V_{SA} = -2.2$V, $I_{Rear\text{-}SGDBR} = I_{Front\text{-}SGDBR} = 0$ mA and SOA section floating: (c) 2D optical spectral map from the rear SGDBR side as a function of gain current where low intensity reflection peaks between the main peaks can be clearly seen; (d) corresponding autocorrelation traces with an average period of 1.4 ps at $I_{Gain} = 280$ mA.

3.2 Performance measured from SOA side with rear SGDBR floating and $I_{Front\text{-}SGDBR} = 0$ mA

Similarly to the second scenario in Section 3.1, in this case the gain and SOA sections were forward biased, while the rear SGDBR was left floating, $I_{Front\text{-}SGDBR} = 0$ mA, and a reverse bias was applied to the SA section. As expected, the rear and front SGDBRs acted as passive filters with longitudinal mode spacings of 640 GHz and 700 GHz respectively, producing

#213508 - $15.00 USD Received 6 Jun 2014; revised 20 Aug 2014; accepted 21 Aug 2014; published 29 Aug 2014

pulse trains at both repetition frequencies simultaneously. Due to the contribution of signals generated in the rear and front SGDBR sections and the nonlinearities primarily in the SA, gain and SOA sections, the device produced much more interesting results, such as ML behaviour at frequencies equal to the sum, or the mean of the designed frequencies of the rear and front SGDBRs, depending on the applied drive conditions.

To explain these phenomena, firstly, nonlinear mixing, due to nonlinearities primarily in the gain, SOA, and SA section with relatively high V_{SA} values, can be described by the following equation:

$$\begin{aligned} s(t) &= f_f(t) \times f_r(t) = A_f \cos(2\pi f_f t) A_r \cos(2\pi f_r t) \\ &= 0.5 A_f A_r \left[\cos\left(2\pi(f_f + f_r)t\right) + \cos\left(2\pi(f_f - f_r)t\right) \right] \end{aligned} \tag{2}$$

where $s(t)$ is the signal from the SOA side facet, f_f (t) and f_r (t) are the front and rear SGDBR ML signals respectively (for simplicity, here we assume they comprised only one frequency component, i.e. sinusoidal signals with frequencies 700 GHz (f_f) and 640 GHz (f_r), respectively), and A_f and A_r are their corresponding signal amplitudes. Due to these modulation effects in the SOA section, the generation of 1.34 THz (i.e. the sum of 700 GHz

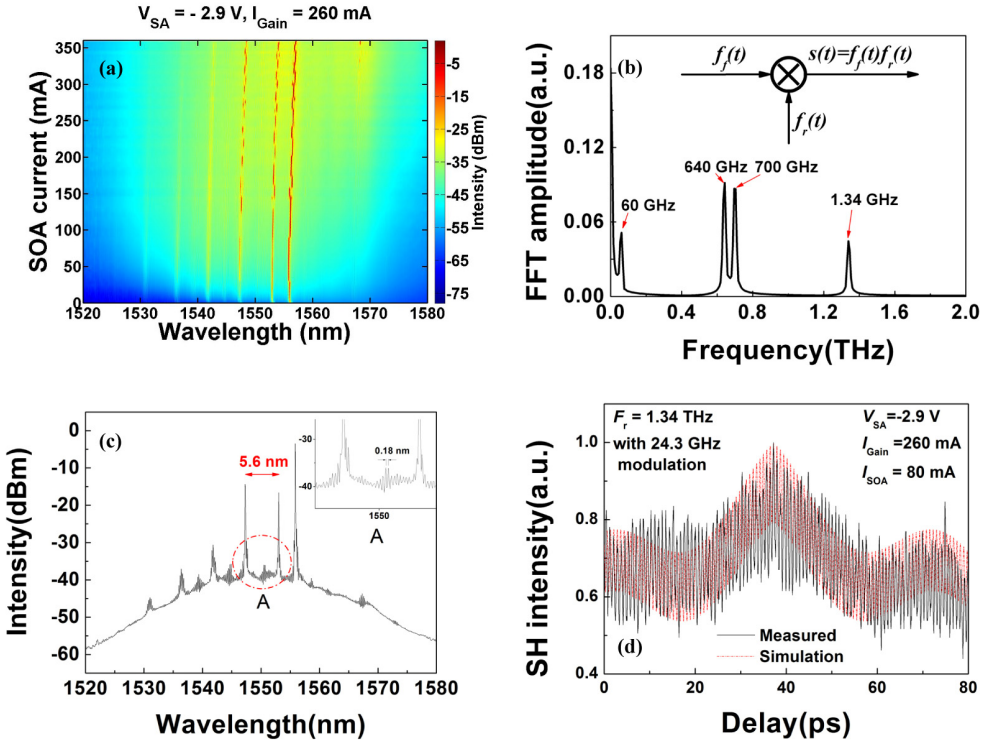

Fig. 5. Device performance measured from the SOA side output facet with $I_{Front\text{-}SGDBR}$ = 0 mA and the rear SGDBR floating: (a) 2D optical spectra from the SOA side as a function of SOA current when V_{SA} = –2.9 V and I_{Gain} = 260 mA, (b) simulated FFT spectrum from Eq. (2), (c) optical spectrum with inset showing the fundamental mode spacing of the 1770 μm long main cavity (0.18 nm), and (d) corresponding measured and simulated autocorrelation pulse train with V_{SA} = –2.9V, I_{Gain} = 260 mA, and I_{SOA} = 80 mA.

and 640 GHz) will also occur, as well as a beat tone at 60 GHz. In practice mixing could be observed over a wide range of bias currents, with the gain and SOA sections pumped, the SA section reverse biased, the front and rear SGDBR weakly positively biased (< 40 mA) or left floating. Observing the output from the SOA output facet, signals at 1.34 THz were observed

#213508 - $15.00 USD Received 6 Jun 2014; revised 20 Aug 2014; accepted 21 Aug 2014; published 29 Aug 2014

with applied V_{SA} values between −3 V and −2.2 V, I_{Gain} between 200 mA and 260 mA, and the SOA bias, I_{SOA} between 0 and 250 mA. These effects are depicted in Fig. 5. A 2-D optical spectral map as a function of the SOA current with V_{SA} = −2.9 V and I_{Gain} = 260 mA is depicted in Fig. 5(a). As shown, the lasing lines were very stable with little red shifting (heating effects) as I_{SOA} was increased from 0 mA to 360 mA.

The mode spacing was defined by the rear and front SGDBR sections, respectively. Since the mode spacing of the two gratings is comparable, it is very hard to distinguish them on the optical spectral map. Figure 5(b) shows the simulated fast Fourier transform (FFT) spectrum derived from Eq. (2). Due to nonlinear mixing between the original 640 GHz and 700 GHz frequencies taking place in the SA and gain sections, we should observe both the sum frequency, 1.34 THz, and the difference frequency, 60 GHz, according to wave mixing rules. The main plot of Fig. 5(c) shows the optical spectrum at V_{SA} = −2.9 V, I_{Gain} = 260 mA and I_{SOA} = 80 mA and the inset shows the fundamental longitudinal mode interval of 0.18 nm or 24.3 GHz of the 1770 μm long main effective cavity is present, close to the simulated value of 0.19 nm in Fig. 2(c). A mode spacing of 5.6 nm is clearly observed and is determined by the front SGDBR corresponding to 700 GHz. The optical spectral peaks defined by the rear SGDBR were not very apparent due to the relatively lower reflectivity, and its further distance away from the measurement facet. However, from the lower level peaks between the main peaks, and by comparison with the simulation of transmission from the SOA side shown in Fig. 2(c) and the net gain for the SGDBR MLL shown in Fig. 2(d), we can conclude that the measured optical spectrum was the product of the reflections from both the front and rear SGDBR sections. The black solid line in Fig. 5(d) shows the measured AC trace of the pulse train from the device operating with V_{SA} = −2.9 V, I_{Gain} = 260 mA, and I_{SOA} = 80 mA. The average period of the pulse train was 0.75 ps, which corresponds to an F_r of 1.34 THz, i.e., the sum frequency.

The expected beat frequency at 60 GHz was not distinctly observable in the measured autocorrelation trace, which may be due to frequency filtering by the rear SGDBR ($\Delta\lambda_{bw}$ ≤110 GHz) [10] removing the two modes of the 60 GHz signal adjacent to the main spectral lines. However, a modulation frequency at ~24.3 GHz was apparent over the entire autocorrelation trace. This is related to the fundamental round-trip frequency corresponding to the 1770 μm cavity length as shown at Fig. 2(a). A simulated AC trace of a pulse train with a 1.34 THz repetition frequency and strong modulation at 24.3 GHz has been overlaid in Fig. 5(d). As clearly shown, the additional 24.3 GHz modulated signal results in a DC offset in the AC trace, agreeing well with experimental observations. We have also modelled the effects of other frequency components that might be present in the pulse train (e.g. 60 GHz). Other frequencies, such as the second (48.6 GHz) and higher harmonics of the fundamental round-trip frequency of the main cavity could be clearly observed under some drive conditions, (akin to the behavior observed and mentioned in the second scenario of Section 3.1). However within the tolerances of this experiment, the presence of just a single additional modulation at 24.3 GHz offers a reasonable fit to the measured results. The DC component as well as the 24.3 GHz envelope modulation could be easily removed using readily available filtering techniques, thus leaving a pure 1.34 THz repetition rate pulse train for use in practical applications.

It is worth noting that besides the simple and practical case with $I_{Front\text{-}SGDBR}$ = 0 mA and the rear SGDBR floating, the device was fully characterized over all operable positive bias currents (0~40 mA) applied to both the front and rear SGDBR sections, and similar phenomena were observed, with the exception of the modulation frequency, (i.e., the fundamental round-trip frequency of the laser cavity length) which decreased as I_{SGDBR} was increased. This frequency reduction with increasing I_{SGDBR} is due to the increase in the effective cavity length caused by the lower absorption loss in the SGDBR sections [10]. Due to the 20 nm redshift of the lasing wavelength compared to the PL wavelength, the saturation absorption effect in the SGDBR section does not seriously affect the ML characteristics of the device, and this is confirmed by our device characterisation results. Moreover, the lasing

#213508 - $15.00 USD Received 6 Jun 2014; revised 20 Aug 2014; accepted 21 Aug 2014; published 29 Aug 2014

peak, λ_{peak}, and mode spacing were determined precisely by Λ and Z_0, respectively. The temperature tuning coefficient of λ_{peak} was< 0.06 nm/K over the range 20°C - 70°C and the mode spacing was essentially independent of temperature. Stable ML over a wide range of drive parameters is a key feature of these lasers.

It is also worth noting that as $|V_{SA}|$ was decreased below 2.2 V and with I_{Gain} > 295 mA and $I_{SOA} \geq$ 250 mA, the optical spectra of the modes defined by the rear and front SGDBRs widened due to self-phase modulation (SPM) in the gain section [15], and the spectra of the 2-3 adjacent modes from the front and rear DBRs overlapped. This allowed ML to take place at the mean frequency defined by the modal interaction between the rear and front SGDBRs as illustrated in the inset of Fig. 6(a). The main plot in Fig. 6(a) shows the 2D optical spectral map from SOA side as a function of I_{Gain} when V_{SA} = –2.1 V, I_{SOA} = 250 mA. Figure 6(b) shows the optical spectrum at I_{Gain} = 300 mA. The central wavelength was 1563 nm with a channel spacing of 5.43 nm and 3 dB bandwidth of 5.27 nm. The spacing of the peak wavelength of the adjacent channels corresponds to a ML repetition frequency of 666 GHz. Figure 6(c) shows the measured AC trace at V_{SA} = –2.1 V, I_{Gain} = 300 mA and I_{SOA} = 250 mA. The average period of the measured emitted pulse train was 1.50 ps, corresponding to F_r = 666 GHz (i.e., close to the mean value of 640 GHz and 700 GHz). Modulation associated with the fundamental and second harmonic round-trip frequencies of the main cavity is also apparent.

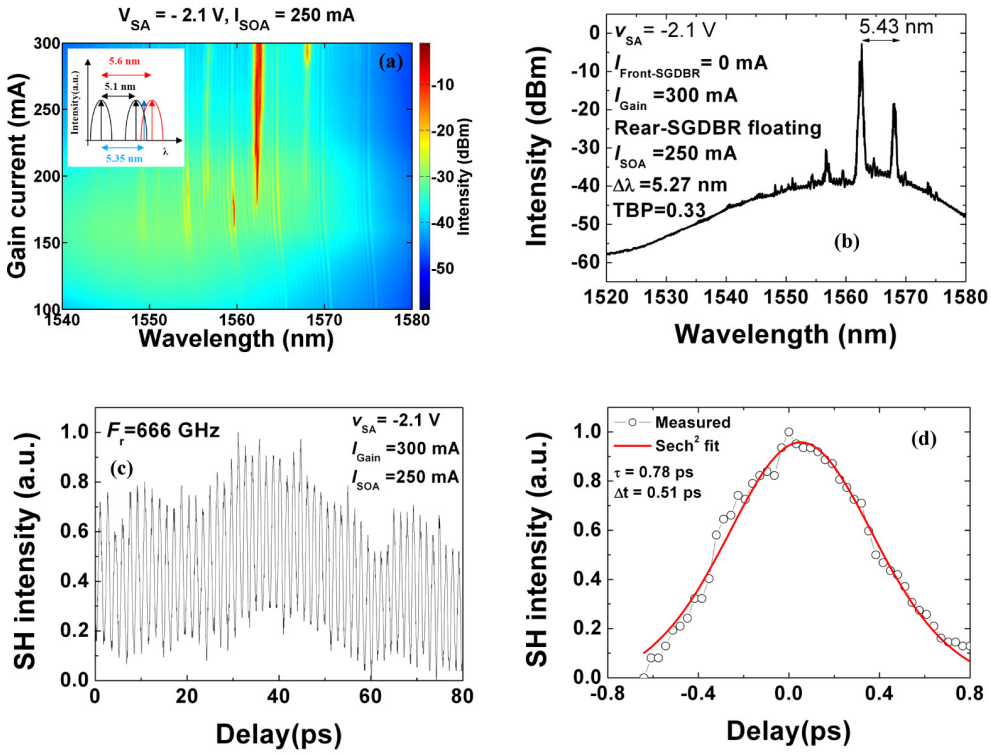

Fig. 6. Device performance measured from the SOA side output facet with V_{SA} = –2.1V, I_{SOA} = 250 mA, $I_{Front\text{-}SGDBR}$ = 0 mA, and rear SGDBR section were floating: (a) 2D optical spectral map from SOA side as a function of gain current where the lasing modes can be clearly seen as high intensity regions, (inset: SPM effects producing the mean frequency defined by the modal interaction between the rear and front SGDBRs), (b) optical spectrum, (c) corresponding autocorrelation traces and (d) an isolated AC pulse fitted in red by a sech^2 pulse shape with a FWHM of 0.78 ps and corresponding deconvolved pulse length 0.51 ps measured at V_{SA} = –2.1V, I_{Gain} = 300 mA, I_{SOA} = 250 mA.

#213508 - $15.00 USD Received 6 Jun 2014; revised 20 Aug 2014; accepted 21 Aug 2014; published 29 Aug 2014

The AC width of an isolated pulse was 0.78 ps, which deconvolves to a pulse width of 0.51 ps, assuming a $sech^2$ pulse shape [Fig. 6(d)]. The time-bandwidth product (TBP) of the pulse is equal to 0.33. The average output power was ~46 mW with a corresponding peak power of 120 mW.

It should be pointed out that during the characterisation measurements, the AC clearly displayed the presence of THz oscillations, which remained stable throughout the measurement procedures with most of the background noise filtered out using appropriate sample averaging. Due to the high repetition frequency of the pulse trains, it is not possible to perform a direct measurement of the radio frequency (RF) characteristics. However, we were able to infer these characteristics by using the well-known coherent heterodyne technique to measure the optical linewidth of individual modes when the laser was mode-locked. When the laser was operated in the 666 GHz and 1.34 THz ML regimes, the RF signal was stable with a linewidth of about 2.0 MHz; on the contrary, when the laser was operating in the incomplete ML or no-ML regime, the RF signal was relatively unstable (i.e. large signal drift) with a linewidth of about 10 MHz. This reduction of a factor of 5 in linewidth provides strong evidence that, in the ML regime, the laser modes are indeed phase-locked [13, 16].

4. Conclusion

In conclusion, we have demonstrated a novel 1.55 μm range AlGaInAs/InP side-wall SGDBR laser with dual DBR gratings, which is monolithically integrated with an SOA. The devices were fabricated using simple first-order sidewall grating technologies, which have the advantage of eliminating crystal regrowth and allow the AlGaInAs quaternary structure to be used in the QW active section. The grating structure also relaxes the fabrication tolerances of the laser, offering considerable advantages over the deep-etched HML method using coupled FP cavities previously reported in [5], and because it is a surface grating, eliminates the need for complex regrowth fabrication steps normally associated with DBR lasers.

A single device can generate mode-locked optical pulse trains at pulse repetition frequencies of 640 GHz, 700 GHz, 666 GHz, and 1.34 THz. The sampled gratings within the rear and front DBR sections provide high finesse optical frequency filtering, creating comb lines separated in frequency by the desired mode-locked frequencies, i.e. 640 GHz, and 700 GHz respectively. By varying the drive conditions, ML operation at the mean frequency of 666 GHz and nonlinear sum frequency (1.34 THz) mixing were observed; further comprehensive modelling studies are underway to provide more detailed insights into these phenomena. Our experimental results show the nonlinearities arise primarily in the gain, SOA, and SA sections with relatively high V_{SA} values. Due to the combination of strong filtering and saturable absorption, the device strongly favours operation in the mode-locked regime, and stable ML is observed over a wide range of bias parameters in terms of drive currents and bias to the gain, SOA and SA sections. These SGDBR lasers are the first to demonstrate ML at pulse repetition rates >1 THz in a device with an operating wavelength of 1.5 μm. Compared with other reported devices, our laser uses a simple and reproducible fabrication technology and exhibits highly controllable and robust mode-locked operation. These laser diodes are expected to open up many opportunities for future compact THz applications.

Acknowledgments

The authors would like to acknowledge financial support from EPSRC (project EP/E065112/1) and the staff of the James Watt Nanofabrication Centre at the University of Glasgow for help in fabricating the devices reported in this paper.